Version of Record: https://www.sciencedirect.com/science/article/pii/S0920379620304804
Manuscript_2ce4fb3b71cb0743e1b7351bc6232778

Error field correction strategies in preparation to MAST-U operation

L. Piron[1,2,3], A. Kirk[3], Y.Q. Liu[3,4], G. Cunningham[3], M. Carr[3], R. Gowland[3], I. Katramados[3], R. Martin[3]

[1]Dipartimento di Fisica "G. Galilei", Universita' degli Studi di Padova, Padova, Italy
[2]Consorzio RFX, Corso Stati Uniti 4, 35127, Padova, Italy
[3]CCFE, Culham Science Centre, Abingdon, OX14 3DB, UK
[4]General Atomics, P.O. Box 85608, San Diego, California 92186-5608, US

E-mail: lidia.piron@unipd.it

June 2020

Abstract.

In magnetic fusion devices, unwanted non-axisymmetric magnetic field perturbations, known as error fields (EF), can have detrimental effects on plasma stability and confinement. Such EFs may originate from several sources, such as axi-symmetric coil misalignments, coil feeds, 3D structures in the wall surrounding the plasma, presence of ferromagnetic materials near the plasma surface, blanket materials in future devices. To minimize their impact on plasma performance and on the available operational space, it is important to identify the EF sources and develop EF control strategies. MAST Upgrade (MAST-U) is a spherical tokamak which will operate in the near future after a series of enhancements from the previous MAST experiment *[Morris A. W. et al, "MAST Accomplishments and Upgrade for Fusion Next-Steps" IEEE Transactions on Plasma Science, April 2014]*. To deliver a machine with EF amplitude low enough to allow a high quality experimental programme, systematic analysis of the intrinsic EF sources has been carried out for poloidal field (P) and divertor (D) coils. To deliver a machine with EF amplitude low enough to allow a high quality experimental programme, systematic analysis of the intrinsic EF sources has been carried out for poloidal field (P) and divertor (D) coils, whose magnetic field measurements were available when writing this paper. Such measurements reveal that P and D coils are 3D deformed and thus are responsible for intrinsic EFs, with mainly n=1 and n=2 toroidal mode numbers. In preparation to MAST-U operation, both passive and active EF control strategies have been adopted for n=1 and n=2 EFs compensation. Passive EF control consisted of installing finely each D and P coil within MAST-U device so as to minimize the intrinsic n=1 EF amplitude. The optimal coil alignment has been determined based on magnetic field measurements and the corresponding 3D electro-magnetic modelling, and envisaged coil shift and tilt of 3.2 mm and 0.7 mrad, respectively, in the case of P coil named P4. Conversely, active control will be use during MAST-U operation to reduce the n=2 EF which is associated mainly with P4 and P5, as well *[Kirk A. et al 2014 Plasma Phys. Control. Fusion 56 104003]*. Since these coils have been re-used from the MAST device, studies attempting n=2 EF control, based on MAST plasmas, have been modelled utilizing the MARS-F code *[Liu Y. Q. et al 2000 Phys. Plasmas 7 3681]* to interpret experimental results in MAST and to give hints for future n=2 EF control studies in MAST-U. A model-based control set for

n=2 EF control has been identified which would allow for the minimization of rotation braking, of the resonant magnetic field at the q=2 and of the plasma displacement in MAST-U, simultaneously.

1. Introduction

In magnetic fusion devices, such as tokamaks, non-axisymmetric magnetic field perturbations can be present. They can be deliberately applied by means of active coils, magnetic coils located in- and/or ex-vessel, for example to control Resistive Wall Modes [1, 2] and Edge Localized Modes [3, 4], or to tailor rotation and rotation shear, a technique demonstrated to improve stability of quiescent-H mode [5]. On the other hand, 3D magnetic fields can arise due to imperfections or misalignment of equilibrium stability control and shaping coils, coil current feeds, eddy currents associated with 3D wall structures and ferritic material located in the vicinity of the plasma. These un-intended 3D fields are known collectively as error fields (EFs).

EFs with amplitude δB as small as $\delta B/B_t \approx 10^{-4}$ (δB, depending on various engineering parameters, such as plasma density and the major radius of the plasma, and B_t being the toroidal magnetic field) can have a large impact on energy confinement and plasma stability in tokamaks [6, 7, 8, 9, 10, 11]. In ITER and DEMO it will be even lower, of about $\delta B/B_t \approx 10^{-5}$, since the EF threshold decreases with increasing machine size.

EFs can affect plasma through several mechanisms. EFs can slow down plasma rotation so as to induce locked modes that often even lead to a plasma disruption [6, 11, 12, 13]. EFs induced flow damping occurs via various channels, e.g. the electromagnetic (EM) torque, the neoclassical toroidal viscosity (NTV) torque [14, 15, 16, 17], EF can be responsible of inducing fast particle losses [18, 19] and triggering ideal-MHD instabilities when exploring high-β regimes [20, 21, 22].

Identification of reliable EF detection methods and determination of robust EF control strategies in present magnetic fusion devices are of vital importance to ensure success of ITER as well as of next generation tokamaks.

In recent decades, in various fusion experiments, ad hoc studies have been performed to identify EF sources and to develop EF control strategies [23, 24, 25, 26, 27, 28, 29, 30, 31, 32, 33, 34, 35, 36, 37, 38, 39, 40, 41, 42, 43, 22, 44]. These strategies, which aim to minimize the EF amplitude to the lowest value according to certain metrics, can involve passive and active EF control.

By passive EF control we mean techniques that can be pursued during the phase of constructing or upgrading a fusion device in order to compensate static, or the DC component of the EFs. For example, in the NSTX experiment a displacement of the central toroidal field coil bundle was a source of the n=1 EF (n is the toroidal mode number) which has been detected by the presence of a locked mode during plasma operations [9]. In particular, the displacement was caused by an electro-magnetic (EM)

interaction between the toroidal field and Ohmic heating coil in NSTX. Passive EF control has been used to compensate this n=1 EF by placing mechanical shims between the toroidal field coil and the tension tube on which the Ohmic heating coil is wound in an attempt to reduce the motion of the toroidal field coil.

However, passive EF control alone is not adequate for compensating EFs that have a time-varying behaviour, i.e. AC components, in addition to cases where the full harmonic content can not be minimized by passive control. Therefore, fusion devices employ active coils to reduce these EFs. Control algorithms, implemented in the plasma control system (PCS), can counteract such perturbations in real-time by magnetic feedback, resulting in active EF control, also often referred to as dynamic EF correction [45].

It is worth mentioning that active EF control is often tuned to cancel out the resonant magnetic field components, despite driving larger, but more benign, non-resonant magnetic field components, as demonstrated in [46, 47, 48].

Active EF control has been applied in several magnetic fusion devices. In NSTX, for example, it has been used to minimize the residual n=1 EF after placing the mechanical shims and to reduce the n=3 EF associated with poloidal field coil manufacturing [9]. In DIII-D, active EF control is run in the PCS to compensate the intrinsic EFs due to the poloidal field coil misalignments and the busbars feeding the toroidal field coils [27, 23, 29]. In RFX-mod, active control has been employed to suppress EFs associated with the presence of a poloidal gap in the wall structure [32, 33]. In MAST, it has been used to reduce the intrinsic n=1 EF associated with the deformation of poloidal field coils [38, 39].

This work presents EF control strategies that have been adopted to compensate the intrinsic EFs associated with divertor (D) and poloidal field (P) coils in MAST Upgrade (MAST-U) device.

MAST-U [49] will be exploited in the near future after a series of enhancements from the previous MAST device. The main new features of MAST-U are 6 new P coils, i.e. P1, PC and PX and P6 coil pairs connected in series, and 14 D coils, i.e. D1, D2, D3, D5, D6, D7 and DP coil pairs connected in series, and a new closed pumped divertor structure which will allow investigation of various divertor configurations, i.e. Super-X, snowflake and long-inner leg. Figure 1 represents a sketch of MAST-U poloidal cross-section, where D and P coil sets are highlighted in blue and in red, respectively.

The presence of EFs in D and P coils has been investigated through high accuracy magnetic field measurements and corresponding 3D EM modelling. Such a study revealed that the main EFs have n=1 and n=2.

It is well known in literature that both these harmonics can interfere with the plasma, limiting the exploration of the available operating space and the achievement of good plasma performance, thus affecting the execution of a high quality experimental programme. For these reasons, EF control strategies, which envisage a modification of MAST-U design and the exploitation of active coils for EF correction, have been investigated to limit the impact of n=1 and n=2 EFs on near future MAST-U operation.

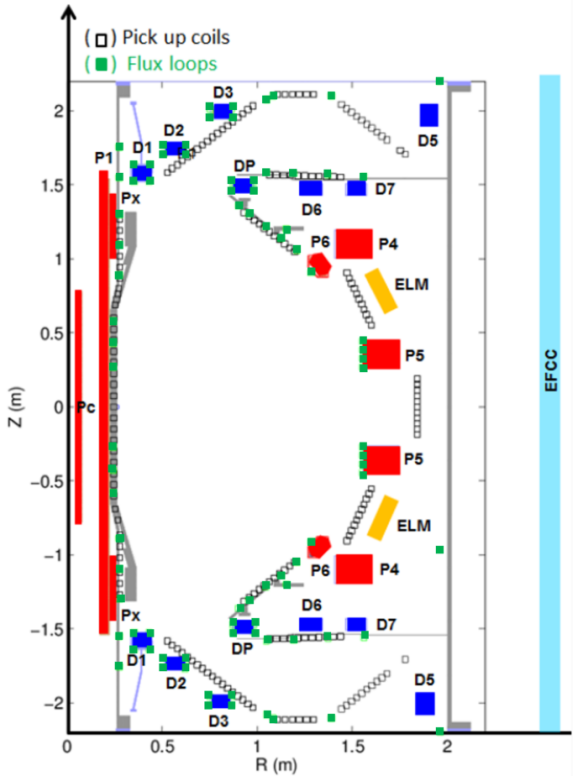

Figure 1. Sketch of the poloidal cross-section of MAST-U device where the P coils are highlighted in red, the D coils in blue, the ELM coils in orange and the EFCCs in light blue. In the same figure, the pick up coils and the flux loops are also reported with black and green squares, respectively.

In particular, passive EF control has been adopted for n=1 EF correction, by identifying the optimal fine-scale coil alignment, i.e. applying coil shift and tilt, in order to minimize the n=1 EF. This is the only EF harmonic that can be compensated in MAST-U due to engineering constrains. We emphasize that this EF compensation strategy deals only with the static n=1 EF.

Conversely, active EF control will be employed for compensating the n=2 EF which is associated with the deformations of P4 and P5. Since these coils have been re-used from the previous MAST device, experiments attempting n=2 EF control, performed during MAST operation, have been investigated through MARS-F [50] modelling to interpret the experimental results and to have hints on active n=2 EF control in MAST-U.

It is worth stressing that this study is not meant to be an exhaustive overview of all the EF sources present in MAST-U. It is based on the analysis of the presently available magnetic field measurements, which allow for pre-emptive EF studies in preparation to next future MAST-U operation, similar to [42]. In the new machine we cannot exclude a priori the presence of other n=1 and n=2 EF sources, besides the ones associated with D and P coils, even with higher toroidal mode numbers and even with a dynamic nature.

To detect other potential EF sources, at the beginning of MAST-U operation, dedicated EF detection studies will be performed. In particular, the compass scan method [51, 52] will be employed. MAST-U, being equipped with an active control system and a wide coverage of magnetic field sensors, is suitable for the compass scan.

The active control system is made up of 2 active coil sets: the error field correction coils (EFCCs) and the edge localized mode (ELM) control coils [31]. These coil sets are represented in figure 1 in light blue and in orange, respectively.

The EFCCs, retained from MAST, consist of four coils arranged symmetrically around the outside of the MAST-U vacuum vessel and are located at R=2.9 m. Each coil is about 4 m high, i.e. -2 m $\leq$ Z$\leq$ 2 m, being made up of 3 turns and can carry up to 5 kA/turn. Each ELM coil spans 0.27 m poloidally by 0.6 m toroidally and is composed of 4 turns, with the available coil current up to 2.1 kA. The actual number of ELM coils has been reduced with respect to MAST (6 and 12, respectively) due to the installation of an off-axis NBI system. Each ELM coil spans 0.270 m poloidally by 0.6 m toroidally and is composed of 4 turns. Due to the upgrade of the ELM coil system, the current power supply limit has been increased from 1.4, the MAST limit, to 2.1 kA.

An extensive coverage of magnetic field sensors, i.e. 398 pick up coils, 102 flux loops, 70 Mirnov and 91 Rogowskis coils, has been installed in MAST-U to detect and control magnetic field perturbations associated with EFs and MHD modes, besides controlling the plasma shape and position and reconstructing the plasma equilibrium. The position of pick-up coils and flux loops is shown, as an example, in figure 1 with black and green squares, respectively. In particular, pick-up coils are located in two toroidal positions, at $\phi = 110$ deg and $\phi = 290$ deg, while flux loops are toroidally continuous.

The paper is structured as follows. Section II presents the methodology adopted to determine the optimal fine-scale coil alignment for n=1 EF compensation in MAST-U. Section III presents MAST experiments with externally applied n=2 magnetic field perturbations. Section IV describes the use of MARS-F code to model based n=2 EF control for MAST-U. Section V gives the summary and the conclusions of the work.

2. Passive n=1 EF control

Within MAST-U project, the strategy to compensate the EFs associated with D and P coil deformations is using the passive EF control during the assembly phase of the machine, rather than correcting them through active EF control during plasma operations.

When constructing MAST-U device, due to engineering constraints, only shifting the coil in both the x and y directions, i.e. x-shift and y-shift of the order of some mm, and tilting it about both the x and y axes, i.e. x-tilt and y-tilt of the order of some mrad, were allowed. The convention for the x, y, z axis direction is indicated in figure 2(a). In this way only the n=1 EF harmonic can be compensated in MAST-U by passive EF control.

The optimal coil alignment for n=1 EF compensation has been identified for each

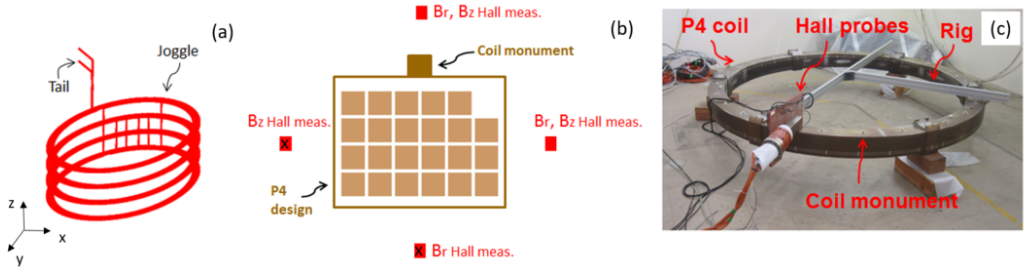

Figure 2. (a) Design of P4 coil, (b) sketch representing P4 coil design cross-section, the position of the coil monument and the position of the Hall probes, (c) picture representing P4 coil, the moveable rig and the Hall probes placed on it.

D and P coil through a methodology which combined magnetic field measurements with 3D EM modelling. In the following, such methodology is reported for a P coil named P4, as an example.

P4 (and P5 as well), retained in MAST-U from the previous MAST experiment, is characterized by the presence of 3D deformations, as demonstrated by magnetic field measurements performed utilizing a rig mounted in MAST vessel [31, 38, 39]. Such coil deformations are associated with the coil design and the manufacturing process.

Generally, a coil is not circularly symmetric even in the coil design because each wire turn has to make a transition from one layer to the next one. These connections are called joggles. The result is that in a coil which is notionally 6 turns by 4 turns, such as P4, its design has only 23 turns, the missing turn being distributed through the coil, as shown in figures 2(a, b). Since joggles introduce a source of non-axisymmetry, EFs are intrinsically present in the design of the coil.

Once the MAST device has been disassembled, new magnetic field measurements of P4 have been performed to characterize its 3D layout. To this aim, 24 coil monuments were welded to the upper surface of the P4 coil case at approximately equal spacings and radius, and a moveable rig fixed the measurement positions of the magnetic field components precisely relative to these coil monuments.

The radial and vertical magnetic field components of P4 coil, i.e. B_r and B_z, have been measured by 3 high accuracy Hall probes mounted in the moveable rig, at the coil monument positions. A picture representing P4 coil, the moveable rig and the Hall probes placed on it is reported in figure 2(c).

Toroidal distributions of a subset of the B_r and B_z measurements, once the Earth's magnetic field has been subtracted, are shown in figures 3(a, b), respectively. The data indicated with dots have been measured by the Hall probes highlighted with a cross in the sketch of figure 2(b), which are about 0.2 m from the coil case, and correspond to P4 fed with 250 A. In the same figure, the corresponding magnetic field distributions calculated by the P4 coil model, described in [38] and identified previously, by the use of a rig mounted in MAST vessel, are reported for comparison and are indicated with

crosses.

Both the data sets have toroidal distributions with a complex structure. The departures from symmetry result from both the geometry of the coil and variation in the (r, z) coordinates of the measurement positions. Therefore, intrinsic EFs with a range of toroidal mode numbers are present in P4 coil.

The methodology for identifying the optimal coil position for n=1 EF compensation combined the new magnetic field measurements, performed in the coil reference frame, with 3D EM modelling.

Because P4 coil case has 3D deformations, both along the radial and vertical directions, the magnetic field measurement positions reported with dots in figures 3(a, b) were not uniformly spaced. Consequently, the magnetic field measurements are not per se useful. It is necessary to represent the coil by some model and then distort the coil model in some fashion to achieve a match to the magnetic field measurements at the actual measurement positions, whose location has been identified by the use of photogrammetry. The reference frame is then arbitrary, but was chosen to be a best-fit plane through the coil monuments positions centred at their centroid.

To describe the 3D coil deformations, a simple single filament coil model has been adopted. The centre of the model coil, whose radius is 1.5045 m, is placed at the coil monument centroid, which defines the (x, y) = (0 m , 0 m), and its vertical position is at z = 0 m. The magnetic field is calculated using the Biot-Savart law at the Hall probe positions and the modelled magnetic field has been compared with the experimental one.

Figures 3(c, d) show the modelled values of the subset of B_r and B_z distributions, highlighted in magenta, together with the corresponding magnetic field measurements, indicated with dots. Note that the modelled magnetic field distributions are not around the mean values of the measured magnetic field components, indicating that the coil is not centred in the coordinate system used to locate the measurements.

Moreover, the modelled magnetic field distributions are not flat. Being in fact calculated at the coil monument positions, the distributions follow the shape of the coil case.

In order to improve the agreement between the modelled and the measured magnetic field components, the single filament has been distorted by radial and vertical displacements with toroidal mode number n up to 12. The radial and vertical coordinates of the coil have been thus expressed as:

$$r = r_0 + \sum_{n=1}^{12} \delta_n^r cos(n\phi) + \sum_{n=1}^{12} \gamma_n^r sin(n\phi), \tag{1a}$$

$$z = z_0 + \sum_{n=1}^{12} \delta_n^z cos(n\phi) + \sum_{n=1}^{12} \gamma_n^z sin(n\phi), \tag{2a}$$

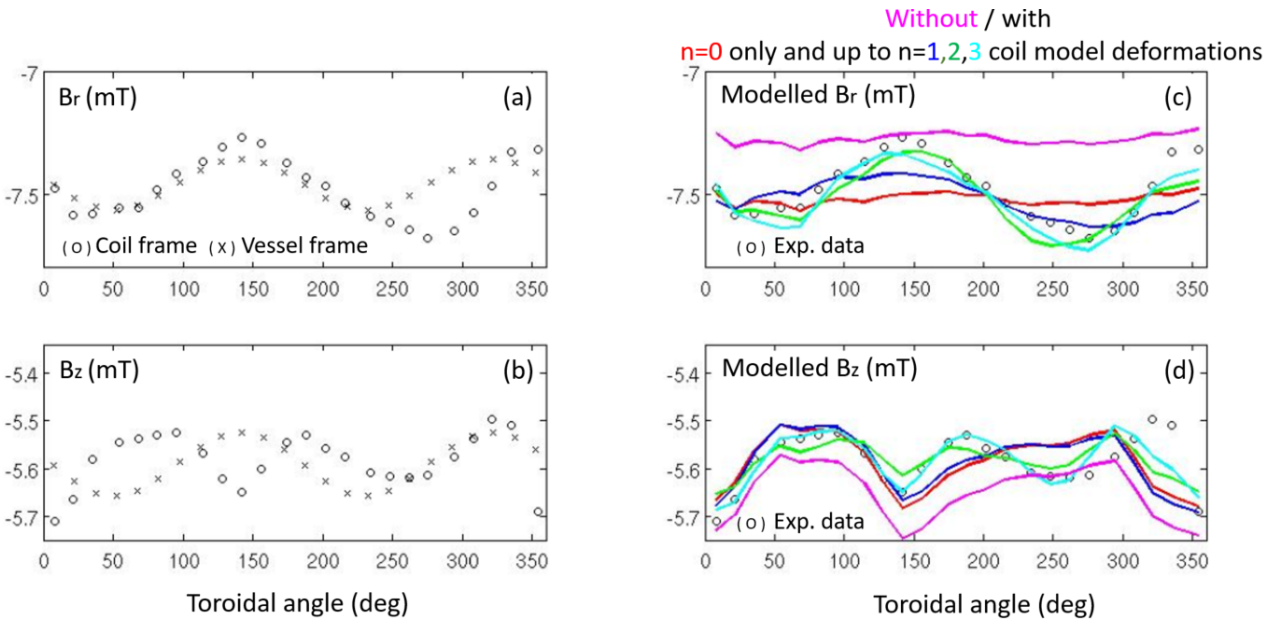

Figure 3. Toroidal distribution of a subset of (a) B_r and (b) B_z measurements in the coil reference frame, indicated with dots, and the corresponding calculated ones, by using the P4 coil model, described in [38] and identified previously, by the use of a rig mounted in MAST vessel, indicated with crosses. Toroidal distribution of (c) B_r and (d) B_z computed at the same positions utilizing a single filament model of P4 coil without deformations (in magenta) and with $n = 0$ (in red), $n = 0, 1$ (in blue), $n = 0, 1, 2$ (in green), $n = 0, 1, 2, 3$ (in cyan) deformations. In these figures, the toroidal distributions of B_r and B_z, acquired in the coil reference frame, are also shown, for comparison.

where r_0 and z_0 represent the radial and the vertical offsets that should be applied to identify the exact coil position, respectively, while the coefficients $\delta_n^r, \gamma_n^r, \delta_n^z, \gamma_n^z$ represent the radial and vertical deformations for each toroidal mode harmonic.

In the simplest case, $\delta_1^r, \gamma_1^r, \delta_1^z, \gamma_1^z$ represent a shift or tilt of the coil and thus produce a toroidal n = 1 asymmetry. The coefficients $\delta_2^r, \gamma_2^r, \delta_2^z, \gamma_2^z$ correspond to a distortion from a flat circle, either in terms of an elliptic or out of plane bowing, and thus produce an n = 2 asymmetry. By increasing n, more complex deformations can be added to the single filament coil model.

The r_0, z_0, $\delta_n^r, \gamma_n^r, \delta_n^z, \gamma_n^z$ parameters, which bring the predicted B_r and B_z into agreement with the magnetic field measurements, have been identified through a non-linear least squares algorithm. The $\delta_n^r, \gamma_n^r, \delta_n^z, \gamma_n^z$ coefficients corresponding to n=1, n=2 and n=3 radial and vertical deformations are reported in figure 4, in blue, green and cyan, respectively. As will be shown later, the dominant components have $n < 3$.

Figures 3(c, d) represent the predicted toroidal distributions of B_r and B_z considering the single filament coil model compensated by radial and vertical offsets, in black, and considering various radial and vertical deformations, indicated with various colors.

To achieve a good agreement between the modelled and the measured magnetic field components, the single filament coil model should accommodate deformations with at least n up to 2, as shown by comparing the magnetic field distributions indicated with a blue line and with dot in figures 3(c, d), respectively. This implies that the P4 coil geometry is characterized by the presence of mainly n=1 and n=2 EFs. A similar conclusion has been drawn previously when magnetic field measurements of P4 (and P5 as well) have been performed in MAST vessel reference frame [31, 38, 39].

The $\delta^r_{n=1}, \gamma^r_{n=1}, \delta^z_{n=1}, \gamma^z_{n=1}$ coefficients have been used, in combination with the toroidal location of P4 tail, to calculate the optimal coil alignment for n=1 EF compensation. Note that the optimal coil alignment has been determined by using a simplified coil model, which takes into account only the n=1 coil deformation accordingly to the magnetic field measurements, thus neglecting the presence of coil tail and joggles.

To assess the importance of including such 3D coil features, the actual P4 design model, shown in figure 2(a), has been used. The predicted adjustment of coil position is very similar to the one computed utilizing the n=1 deformed single filament coil model.

Similar adjustment of coil position for n=1 compensation has been obtained, despite the use of different coil models, because joggles and the coil tail are features very localized toroidally in P4 coil design. In this case, high-n harmonic deformations should be used to describe them. The coil position alignment, being focused on the n=1 EF harmonic only, is not altered by these high-n harmonics.

The optimal adjustment of the coil alignment for n=1 EF minimization in MAST-U has been thus identified by the methodology above described and required relatively small coil shifts and tilts, i.e. x-shift =-2.2 mm, y-shift=3.2 mm, and x-tilt=-0.6 mrad, y-tilt=0.7 mrad, respectively. Clamps have been adopted to finely position and rotate P4 inside MAST-U device and, once the coil has been installed in the lower midplane of the machine, the coordinates of the coil monuments have been rigorously checked by photogrammetry.

It should be stressed that this coil alignment is only optimal for compensation of the static n=1 EF. We cannot exclude a priory that the n=1 EF, associated with P coil deformations, and D coil as well, has a time-varying nature. Dedicated experiments in MAST-U have been planned to access its role and, if its amplitude would not be negligible, dynamic EF correction by means of EFCCs and ELM coils will be employed.

3. Active n=2 EF control

In preparation for the exploitation of MAST-U, the development of a proper control strategy for the n=2 EF is as important as for the n=1 EF since in tokamak devices, such as DIII-D and EAST, similar levels of plasma rotation braking and performance degradation have been observed for n=1 and n=2 magnetic field errors [53, 54, 55, 56, 57, 58, 59].

The first attempt of n=2 EF correction has been performed during MAST operation and allowed us to investigate the effect of external n=2 magnetic fields on plasma

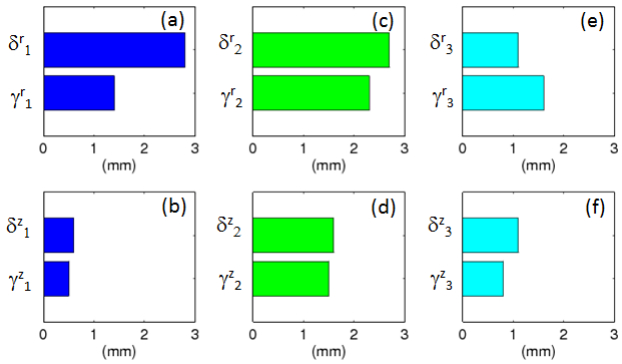

Figure 4. $\delta^r_n, \gamma^r_n, \delta^z_n, \gamma^z_n$ coefficients considering n=1 (a-b), n=2 (c-d) and n=3 (e-f) radial and vertical deformations in P4 coil model.

dynamics and to acquire expertise on n=2 EF control for future experiments in MAST-U.

The metrics we used in this work to assess the effectiveness of n=2 EF control strategy is the avoidance of toroidal braking. In tokamak devices, the sustainment of plasma rotation is beneficial for the plasma through various mechanisms, such as passive MHD stabilization, magnetic screening effect, turbulence suppression [53].

First experiments with externally applied n=2 3D magnetic fields in MAST have used the EFCCs system and were originally designed for ELM suppression and control studies.

Although this topic is beyond the scope of the present work and the database available is limited, these experiments are interesting per se since they allowed to study the effect of external n=2 magnetic field perturbations on the plasma performance and they showed that the EFCCs system is not suitable for n=2 EF correction.

Figure 5 presents three $I_p = 0.7$ MA single null divertor (SND) plasmas. Notably, the time evolution of the main plasma parameters is reported, i.e. plasma density, n=2 EFCC current, D_α emission, Mirnov and Saddle B_r signals, situated on the outboard side of MAST, and core toroidal rotation from change recombination spectroscopy diagnostic (CXRS). The traces in black correspond to the reference plasma where the intrinsic n=1 EF has been controlled by the ELM coils (not shown) [38, 39]. Conversely, the traces in red and in blue refer to plasmas which have, in addition, n=2 magnetic field perturbations applied by means of EFCCs.

The EFCCs system, being equipped with 4 coils and 2 powers supplies, enabled us to set two n=2 magnetic field configurations. In particular, in the experiments presented here, the associated 3D magnetic fields have the same amplitude but a 90 deg phase shift. The corresponding EFCC current is reported in figure 5(b).

Before the application of the external n=2 magnetic fields, the three discharges are similar. Afterwards, the plasma performance degrades in the discharges with external n=2 magnetic fields as demonstrated by the reduction of plasma density and plasma rotation, reported in figure 5(a) and in figure 5(f), respectively.

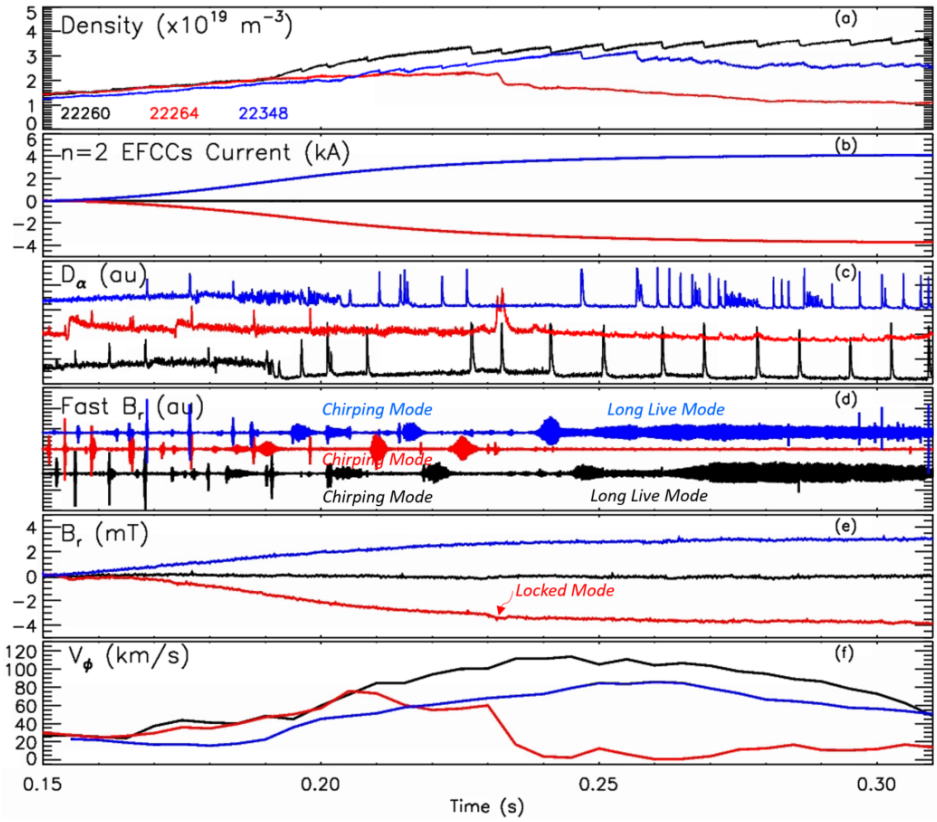

Figure 5. Time behaviour of (a) electron density, (b) n=2 EFCC current, (c) D_α, (d) Mirnov B_r signal, (e) the radial field component of the magnetic field determined from a saddle coil, at the vacuum vessel on the outer mid-plane of the machine, (f) core toroidal rotation at R=1.2 m of the reference plasma (in black) and of plasmas with n=2 magnetic field perturbations induced by negative (in red) and positive (in blue) EFCC currents.

The effect of external magnetic field on plasma dynamics is more dramatic in the discharge highlighted in red. In this case, during the penetration phase of the external magnetic field perturbation, because of the reduction of plasma density, the H-mode access is inhibited, as shown in figure 5(c). Beside this, the core toroidal rotation at around t= 0.23 s is drastically reduced with respect to the reference plasma because of the triggering of a locked mode, whose signature can be seen in the time behavior of B_r, measured from a saddle coil, located at the vacuum vessel on the outer mid-plane of the machine, reported in figure 5(e).

Because of the 0.005 s time resolution of CXRS diagnostic, it is not straightforward to untangle if the rotation slowing down is associated with the locked mode, or if the locked mode is triggered because of the decrease of magnetic shielding effect by plasma rotation associated with the external n=2 magnetic field perturbation. Further investigations on this topic are ongoing and will be reported in a separate paper.

On the other hand, the discharge highlighted in blue, similarly to the reference plasma, is able to access the H-mode regime, as shown in figure 5(c), and a transition

from the chirping mode to the long live saturated mode activity [60] is observed in the Mirnov signal, as reported in figure 5(d). However, rotation braking of about $30-40\%$ with respect to the reference plasma has been observed. The effect is localized in the core, not at the edge (not shown), as in other tokamak experiments [53, 62, 63].

The fact that the application of n=2 magnetic field perturbations induces a braking of plasma rotation, whatever EFCCs magnetic field configurations used, demonstrates that the EFCC system is not suitable for compensating the intrinsic n=2 EF in MAST. Consequently, ELM coil system has been exploited when attempting n=2 EF control.

The n=2 EF control strategy has been developed for various MAST plasma scenarios. The one reported here corresponds to a Ip = 0.6 MA, Bt = 0.44 T SND plasma. The SND configuration has been chosen as scenario where attempting n=2 EF control since the n=1 EF correction by means of EFCCs was well established [38, 39]. The SND plasma, being shifted downward, the lower ELM coils row only has been employed.

Since in the lower row there are 12 ELM coils, various n=2 magnetic distributions can be applied (i.e. relative to the machine co-ordinates). To guide n=2 EF control experiments, the ERGOS code [61] has been used. ERGOS is an EM modelling tool which solves the Biot-Savart law given a realistic description of P4 and P5 coils [38], the source of MAST intrinsic EF, the EFCCs and ELM coils geometry and the current polarity connections among the active coils. It calculates the associated 3D magnetic fields, it adds them together according to the current level in each coil and finally it combines them with the plasma equilibrium field.

The toroidal distribution of the radial magnetic field pattern that should be n=2 compensated by the ELM coils is shown in figure 6(a) in black. This quantity has been calculated by the ERGOS code considering the magnetic fields associated with P4 and P5 coil and EFCCs geometry and the corresponding active coil connections [38] and corresponds to the intrinsic EF n=1 corrected by the EFCCs at R=1.45 m and Z=0 m.

The minimization of the resonant magnetic field of the intrinsic EF, b_{res}, at the q=2 surface has been chosen as EF optimization criterion. It is worth stressing that with the ERGOS code being based solely on an EM model, this EF optimization criterion is valid in the vacuum approximation.

Various ELM coil control parameters have been tested in ERGOS looking for the n=2 magnetic field perturbation which has the optimal amplitude and phase for minimizing b_{res} at q=2. Notably, the ELM coil current, I_{ELM} has been varied within a restricted range, considering the following values I_{ELM} (kA) = [0.5, 1, 1.2]. On the other hand, the ELM coil phase, ϕ_{ELM}, which represents the toroidal phase shift of the n=2 magnetic field perturbation with respect to the location of sector 1 in MAST [38] has been scanned within 0 deg $< \phi_{ELM} <$ 180 deg because of the n=2 periodicity. Such ELM coil control parameter can be adjusted changing the current polarity distribution in the lower ELM coils row.

ERGOS simulations suggest that I_{ELM}=0.5 kA and ϕ_{ELM} = 120 deg are the optimal ELM coil parameters for reducing b_{res} at q=2 in vacuum approximation. This is

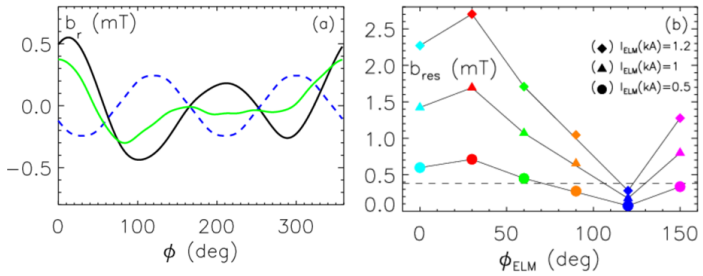

Figure 6. ERGOS vacuum modelling: (a) toroidal distribution of the radial magnetic field, at R=1.45 m, Z=0 m, associated with the n=1 compensated intrinsic EF by means of EFCCs (in black), the optimal (in blue) ELMs coil alignment for the minimization of the resonant radial magnetic field amplitude at q=2, the residual EF amplitude once compensated for both the n=1 and n=2 EFs (in green), (b) resonant radial magnetic field amplitude at q=2 as a function of ϕ_{ELM} and at various I_{ELM}. In this panel, the resonant radial magnetic field amplitude at q=2 without any currents in ELM coils is represented with a dotted line.

shown in figure 6(b) which represents how b_{res} at q=2 scales as a function of the toroidal phase of the external n=2 magnetic field, for different ELM coil current amplitudes. Various colors have been used to distinguish different ϕ_{ELM}, while various symbols have been used to highlight different I_{ELM}.

By the use of I_{ELM}=0.5 kA and ϕ_{ELM} = 120 deg for n=2 EF control in combination with n=1 EF control by means of EFCCs, ERGOS modelling foresees a reduction of the intrinsic EF amplitude with respect to the case with n=1 EF compensation, only. This is shown in figure 6(a), where the toroidal distribution of the radial magnetic field, at R=1.45 m and Z=0 m, associated with the above mentioned quantities are reported in green and in black, respectively.

It is important to point out that the n=2 EF control strategy and the predicted reduction of the intrinsic EF amplitude by means of multi n-EFs control have been obtained using the vacuum approximation. In presence of plasma, such conclusions may differ, as demonstrated by experimental and modelling studies carried out in DIII-D and NSTX devices [46, 47, 48]. Such studies have shown, in fact, that vacuum approach is invalid for calculating fields on resonant surfaces. Magnetic field components that can excite the q=2 resonance in vacuum can be strongly reduced when plasma response is included, and the magnetic field at q=2 is generated by higher m magnetic field harmonics at the plasma boundary (m is the poloidal mode number).

To test the validity of ERGOS predictions, dedicated experiments have been performed during MAST operation. It is worthable stressing that the time dedicated to this study has been limited: 4 shots only have been performed varying the ELM coil control parameters, while correcting the n=1 EF through the EFCCs system as in [24]. The density is not kept the same in all discharges, due to different initial fuelling conditions, so a straightforward comparison on the plasma performance can not

Table 1. ELM coil control parameters for n=2 EF control tested in the discharges reported in figure 7.

Shot	I_{ELM} (kA)	ϕ_{ELM} (deg)
30005	0	0
29916	0.5	120
29915	1	120
30130	0.5	30
30128	1	30

be carried out. Despite this aspect, these discharges have been reported here because they represent the first attempt on n=2 EF control in MAST and through MARS-F modelling, described in the next section, allow us to have hints for future n=2 EF correction studies in MAST-U.

The experiments which aimed at n=2 EF control are reported in figure 7. The traces indicated in black refer to the reference plasma, i.e. the plasma with n=1 EF control by means of EFCCs only. The other traces correspond to plasmas which have in addition various externally applied n=2 magnetic field perturbations by ELM coils whose control parameters are listed in table 1. In particular, the discharges highlighted in cyan and in green used $\phi_{ELM} = 30$ deg. Conversely, the discharges plotted in blue and in red have $\phi_{ELM}= 120$ deg.

In all the experiments, 4 MW NBI power (not shown here) has been injected starting from t=0.1 s, which sustains plasma rotation due to beam trapping and the subsequent coupling of energy and momentum to the plasma.

Before the application of the external n=2 magnetic field perturbation, around t=0.25 s, the core rotation is similar among the plasmas, as shown by comparing the corresponding traces reported in figure 7(f). Afterwards, similarly to the experiments where n=2 magnetic field perturbations have been applied by EFCCs, a rotation braking has been observed.

In particular, in the discharges reported in red, cyan and green, after some plasma momentum diffusion times, of about t = 0.1-0.15 s, the core rotation is reduced by about $60 - 70\%$ with respect to the reference plasma and a consequent degradation of the plasma performance have been observed, as shown in the time behavior of plasma density and D_α emission of discharges reported in red, cyan and in green in figure 7(a) and in figure 7(c), respectively.

It is worth mentioning that in these discharges, a locked mode is triggered. The time instant where a locked mode is observed in B_r signal is indicated with a dotted line in figure 7(f). As in the experiments with n=2 3D magnetic fields by means of EFCCs, the locked mode could be triggered by a partially uncompensated n=1 EF or by the decrease rotation shielding effect due to the external n=2 magnetic field perturbation. Studies on this topic are ongoing and will reported in a separate manuscript.

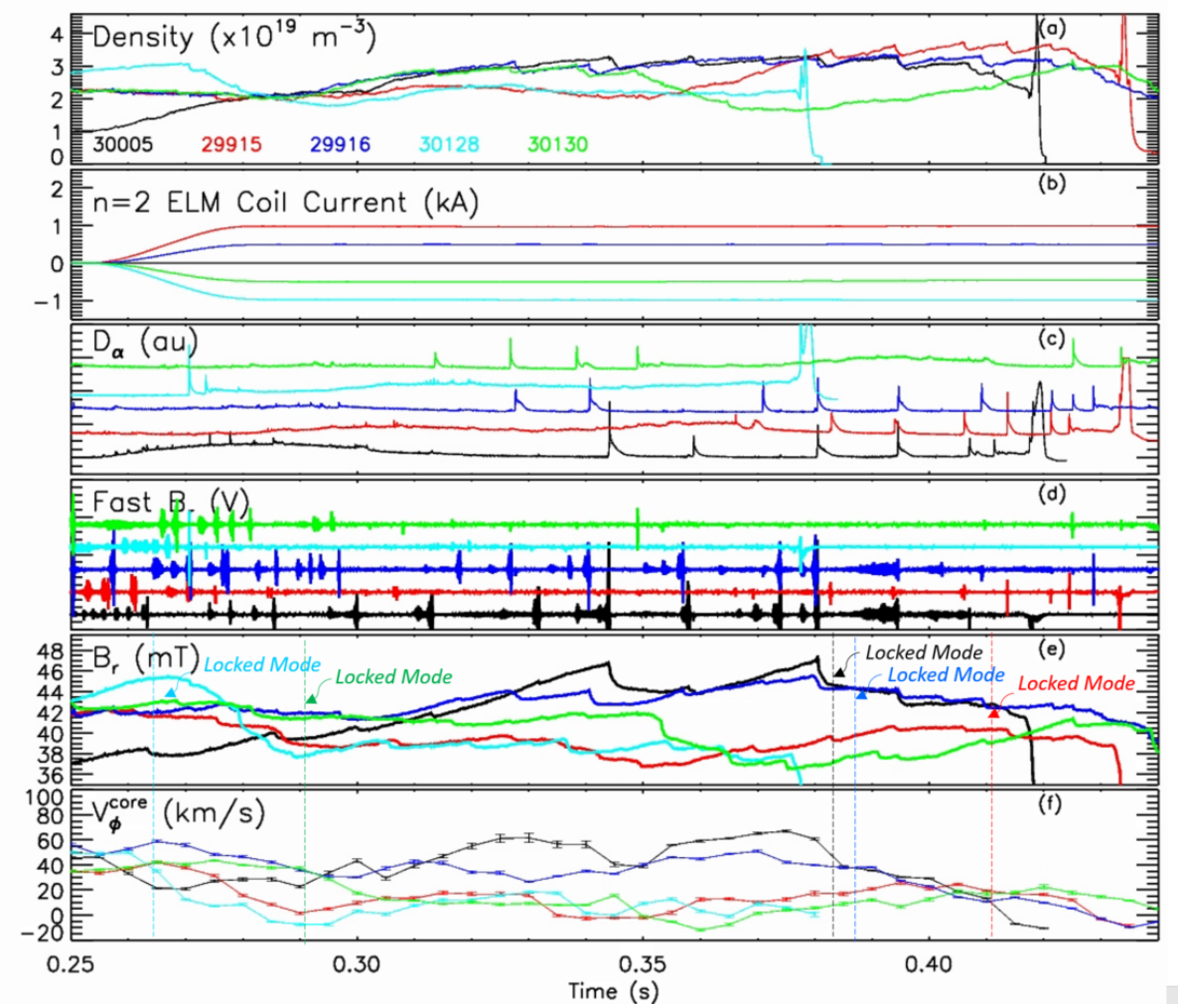

Figure 7. Time behaviour of (a) electron density, (b) n=2 ELM current, (c) D_α, (d) Mirnov B_r signal, s (e) the radial field component of the magnetic field determined from a saddle coil (f) core toroidal rotation at R=1.2 m and the corresponding error bars. The traces in black correspond to the reference plasma, the other traces to discharges various n=2 magnetic field perturbations externally applied by means of ELM coils. The ELM coil control parameters used in these plasmas are summarized in table I.

Conversely, the discharge in blue, among the experiments with externally applied n=2 magnetic fields, has the lowest rotation braking, which is of about $10-20\%$ with respect to the reference plasma. Despite this reduction of plasma rotation, the plasma dynamics is similar to the reference plasma, as shown by the time behavior of plasma density, D_α and MHD activity reported in figures 7(a, c, d, e). As in the reference plasma, around t=0.38 s, a locked mode is triggered. In this discharge, for n=2 EF control, the optimal ELM coil control set, predicted by ERGOS modelling, has been applied.

The fact that a rotation braking has been observed even when using such ELM coil control set demonstrates that a reduction of the intrinsic n=2 EF has not been

achieved. This confirms that vacuum modelling is not suitable for designing n=2 EF control studies, confirming [46].

Actually, MARS-F modelling including the plasma response, carried out after performing these experiments and presented in details in the next section, revealed the ELM coil control set that should have been used for n=2 EF correction, considering various n=2 EF optimization metrics, differs from the one predicted by ERGOS simulations. The optimal n=2 EF control set would only be identified empirically if a finer ELM coil control parameter scan has been performed during the n=2 EF control experiments. Unfortunately, such a detailed scan has not been carried out due to the limited experimental time available in MAST for this study.

4. Optimization of n=2 EF control based on MARS-F modeling

The MARS-F code is a linear single fluid MHD code, in full toroidal geometry, that combines the plasma response with the vacuum perturbations, including the screening effects due to toroidal rotation.

This code has been used in [39] to understand which control criteria the optimal n=1 EF control strategy, empirically identified, fulfils. In this work, the MARS-F code has been used to interpret the experimental results on n=2 EF control and to guide n=2 control parameters for future MAST-U experiments.

The 29916 discharge has been chosen for this modelling study since it has the lowest rotation braking among the n=2 EF control experiments. The corresponding plasma equilibrium at t=0.35 s has been computed by EFIT code, which has been then truncated and re-solved by the CHEASE fixed boundary equilibrium solver [65]. In this case, a static equilibria, as CHEASE computed, has been used since the plasma rotation frequency is well below sound wave frequency, i.e. the Mach number is about 0.16. The flow correction to equilibrium has been thus not taken into account.

Similar to [39], the intrinsic n=2 EF associated with the P4 and P5 deformations is represented by an equivalent surface current in the MARS-F code. By defining this quantity we are able to study the response of the plasma to the intrinsic n=2 EF. Since we are interested in n=2 EF control, this single toroidal harmonics is included in the study. The EF control problem is treated linearly, so there is no coupling between the intrinsic n=1 and n=2 EFs which can be separately investigated without affecting the final computational results [39].

For the calculation of the equivalent surface current, the MARS-F code requires as input the normal magnetic field of the n=2 EF source. This quantity has been calculated by the ERGOS code. Figure 8 shows the plasma boundary and the surface where MARS-F calculates the equivalent current source, plotted in red and in blue, respectively.

In MARS-F simulations, the combination of the intrinsic n=2 EF and the ELM magnetic fields has been considered, aiming at identifying the ELM coil control parameters which minimize the target quantity according to a certain criterion. In the

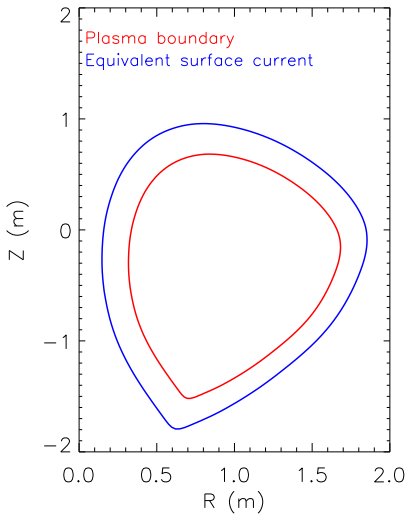

Figure 8. Plasma boundary (in red) and the surface where MARS-F computes the equivalent current source (in blue). The quantities refer to 29916 discharge at t=0.35 s, time instant of EFIT plasma equilibrium calculation.

following, the n=2 EF optimization criteria, investigated through MARS-F modelling, are briefly described.

- Full cancellation of the n=2 resonant magnetic field

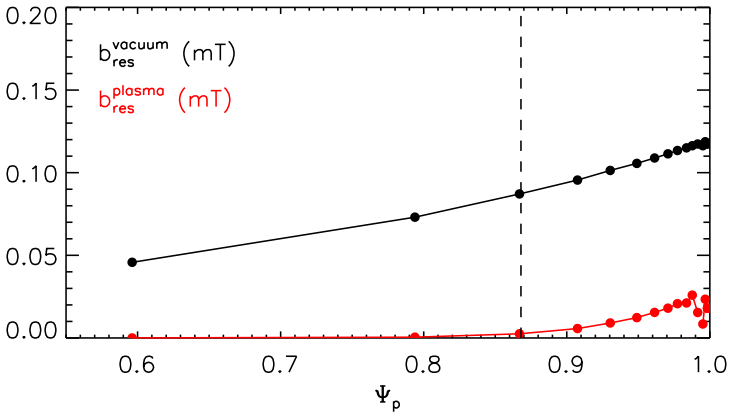

Figure 9. Resonant components of the vacuum field (in black) and the full field including the plasma response (in red) predicted by the MARS-F modelling. The position of q=2 is indicated with a dotted line.

Similar to [38, 39], we have investigated the ELM coil control parameters which cancel the resonant n=2 magnetic field, obtained summing the EF and the ELM field. The resonant n=2 magnetic field should be nulled either at a certain magnetic field surface or its mean value, considering either the cancellation of the vacuum

field only and that of the full field, which includes also the plasma response.
In this n=2 EF optimization criterion, the main poloidal mode number we are interested in is the m=4, which can resonate at the q=2 surface, location of a strong plasma instability [66, 67]. The application of n=2 magnetic field perturbations by means of ELM coils induces a wide spectrum of poloidal harmonics. In principle, the m=3 and the m=5 mode numbers should be also investigated in this study but the 3/2 and the 5/2 MHD modes have never been a concern during MAST operation. For this reason, the cancellation of the resonant field at the q=2 has been reported here while futher investigations on the poloidal spectrum produced by ELM control coil set, and EFCC set as well, will be reported in a separate contribution.
Figure 9 shows the resonant n=2 radial magnetic field components as a function of ψ_p, the normalized equilibrium poloidal flux, in vacuum approximation, in black, and including the response of the plasma, in red. In vacuum approximation, the n=2 resonant magnetic field is small in the plasma core, compared to that near the edge. With the inclusion of the plasma response, the resonant field amplitude is significantly reduced everywhere inside the plasma. This is mainly due to the strong shielding effect coming from the fast toroidal plasma rotation which is about 5% of the Alfvén speed.

- Minimization of the 3D plasma distortion

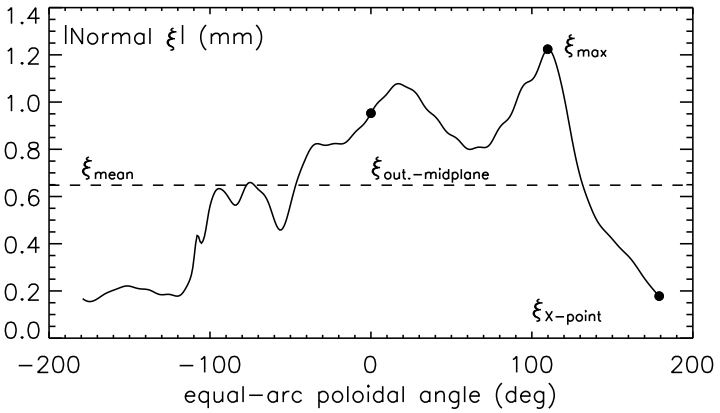

Figure 10. Normal displacement of the plasma surface as a function of the poloidal angle in straight-line coordinate predicted by the MARS-F code. Different metrics for the minimization of the plasma displacement are also highlighted, i.e. the mean displacement, the maximum displacement, the displacement near the X-point and the outboard midplane displacement.

Several experiments have shown that the presence of non-axisymmetric magnetic field perturbations can cause a 3D deformation of the plasma boundary [72]. 3D plasma displacement can have detrimental effects on the plasma, such as triggering the density pump-out [69, 71, 70] and increasing the plasma-wall interaction. It

is thus important to reduce the 3D plasma deformation to the lowest possible amplitude.

We can define various metrics for this criterion which aim to minimize the 3D plasma distortion, namely the maximum amplitude of the displacement along the poloidal circumference, ξ_{max}, the average amplitude of the displacement, ξ_{mean}, the outboard midplane displacement, $\xi_{out.-midplane}$, and the displacement near the X-point position, $\xi_{X-point}$.

All these metrics are represented in figure 10, which shows the normal displacement of the plasma surface as a function of the poloidal angle in straight-line coordinate. The displacement is higher around $\theta = 110$ deg because the lower ELM coils row have been used for n=2 EF control in the plasma modelled. The displacement is also large around $\theta = 0$ deg because of the kink-ballooning.

- Minimization of the net total torque

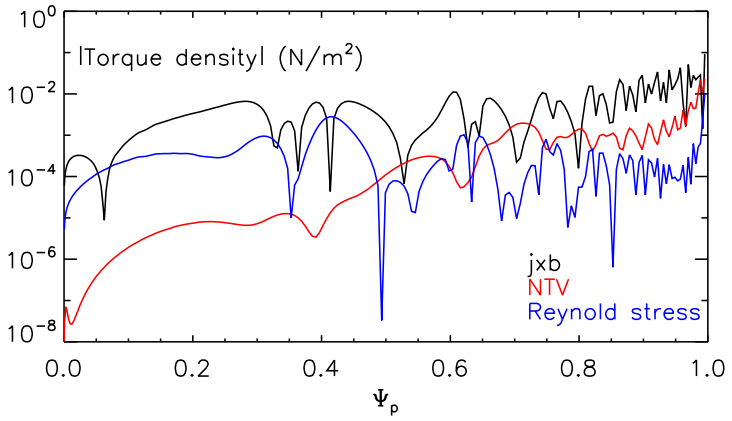

Figure 11. Comparison of various toroidal torques density, i.e. the resonant EM j×b torque (in black), the NTV torque (in red) and the torque due to the Reynold stress (in blue).

In MAST n=2 EF control experiments, a braking of core rotation has been observed. In tokamak devices, the sustainment of toroidal plasma rotation is important, as the toroidal flow and its radial gradient can significantly impact plasma confinement and stability. It is thus reasonable to consider the minimization of the total torque acting on the plasma as n=2 EF optimization criterion.

The torques responsible for the rotation braking have been investigated by MARS-F code considering in the momentum balance equation the resonant j×b EM torque, the NTV torque and the Reynolds torque. The j×b torque is associated with shielding currents arising at the resonant surfaces, the NTV results from the toroidal drag force experienced by the plasma particles moving along field lines distorted by the magnetic field perturbations [73, 46], the Reynolds torque is linked to the plasma inertia, the perturbed velocity and the field line stochastization induced by the external magnetic field [74].

Figure 11 compares the computed radial distributions of the jxb, the NTV and the Reynolds torque densities, considering the plasma response to the combined field, i.e. intrinsic EF + ELM coils.

MARS-F foresees that the resonant j×b torque plays a major role in the momentum balance equation in the modelled plasma being about one and two order of magnitude larger than the NTV and the Reynolds torques, respectively.

Since there are several rational surfaces for n=2 response and the rotation braking is not a localized effect, we have used, as criterion for n=2 EF correction, the net total torque across all these surfaces. Here the net total torque refers to the total torque integrated across the whole plasma minor radius.

To identify the ELM coil control parameters which allow for the minimization of each n=2 EF optimization criterion, MARS-F simulations have been performed. Notably, the ELM coil current and the ELM coil phase have been scanned the amplitude and the toroidal phase of the external n=2 magnetic field perturbation varying in the range I_{ELM}=[0, 2] kA, with a variation step of 0.1 kA, and $I\phi_{ELM}$ in the range $\phi_{ELM} = [0, 180]$ deg, with a variation step of 10 deg. In the following, examples of this modelling study are reported.

Figure 12(a) shows how b_{res} at q=2, in vacuum approximation, varies changing the ELM coil control parameters. Since such n=2 EF optimization criterion has been also investigated by the ERGOS code when designing n=2 EF control experiments, ERGOS and MARS-F predictions can be compared. Notably, MARS-F modelling suggests a minimum of b_{res} at q=2 for I_{ELM}=0.3 kA and $\phi_{ELM} = 120$ deg, indicated with a white cross in figure 12(a); on the other hand, ERGOS modelling foresees a minimum of b_{res} at q=2 for I_{ELM}=0.5 kA and $\phi_{ELM} = 120$ deg, based on the limited ELM coil control parameter scan presented in figure 6(c).

Note that a good agreement between the codes can be found on the prediction of the optimal ϕ_{ELM} for the minimization of b_{res} at q=2, but a different optimal I_{ELM} is foreseen. The reason of such a discrepancy is due to the fact that a rough I_{ELM} scan has been carried out utilizing ERGOS code. A detailed I_{ELM} scan, performed after n=2 EF control experiments by the use of ERGOS code, confirmed that the use of I_{ELM}=0.3 kA and $\phi_{ELM} = 120$ deg are the optimal ELM coil control parameters for the minimization of b_{res} at q=2, confirming MARS-F prediction. This clarifies the apparent discrepancy on the I_{ELM} prediction among ERGOS and MARS-F codes.

However, the vacuum approximation is not suitable when modelling EF control experiments because plasma shielding, amplification, coupling effects are neglected in this case [46, 47, 48]. For this reason, various n=2 EF optimization criteria, which take into account the full magnetic field, have been investigated.

Change of b_{res} at the q=2 surface, including the plasma response, whilst varying ELM coil control parameters is reported in figure 12(b). The position of the minimum b_{res} in the ELM coil control space is represented with a white cross in this figure. Note that the position of such a minimum differs from the one foreseen in vacuum approximation.

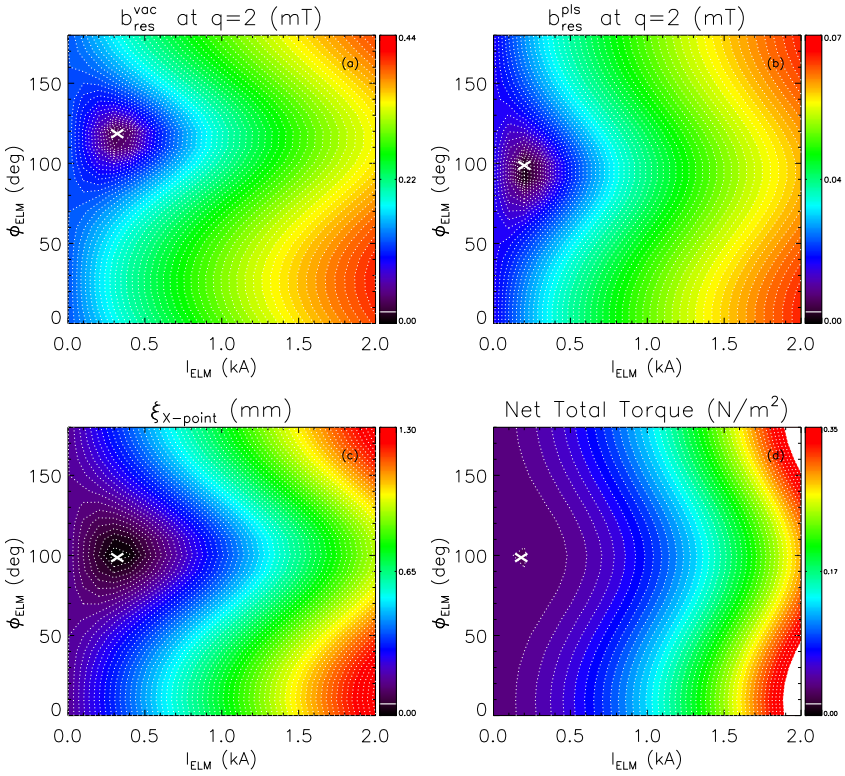

Figure 12. MARS-F modelling: contour plot of (a) the resonant radial magnetic field at the q=2 magnetic surface in vacuum approximation and (b) including the plasma response, as well, (c) the X-point displacement and (d) the net total torque in the ELM coil control space. The cross indicates the optimal ELM coil control parameters for the minimization of each n=2 EF optimization criterion.

Figure 12(c) shows how the X-point displacement varies changing the ELM coil control parameters. The trend is quite similar to that one considering the minimization of b_{res} at q=2 in presence of plasma.

Figure 12(d) represents the contour plot of the net total torque in the ELM coil control space. Such torque is mainly associated with the jxb term in the momentum balance equation. The NTV torque and the Reynold stress torque amplitudes, varying the ELM coil control parameters, have in fact negligible amplitude with respect to the jxb one.

Note that the ELM coil control parameters for the minimization of the net total torque, i.e. I_{ELM} = 0.2 kA and ϕ_{ELM}=100 deg, indicated with a white cross in 12(d), are quite similar to the ones foreseen for the minimization of b_{res} at q=2 and of X-point displacement.

Beside the optimization criteria just described, the minimization of the mean resonant magnetic field including the full magnetic field, the minimization of the mean displacement, its maximum value, and the midplane displacement have been also considered in this MARS-F modelling study.

The ELM coil control parameters of all the n=2 EF optimization criteria investigated are summarized in figure 13 with different colors, while the symbols are used to distinguish different EF minimization metrics within a certain criterion. In the same figure, the ELM coil control parameters used in n=2 EF control experiments are indicated with black dots, for comparison.

MARS-F modelling suggests a narrow region in the ELM coil control space which can satisfy the various n=2 EF optimization criteria investigated. The fact that similar ELM coil control parameters are foreseen by MARS-F for various n=2 EF optimization criteria suggests a synergy among them. This is to be expected as b_{res}, the rotation and the plasma displacement are linked to each other. The resonant radial magnetic field should be minimized to sustain the rotation, the jxb torque being mainly responsible for the rotation braking. It is important to sustain the rotation since MARS-F modelling studies, carried out for both MAST and ITER plasmas, have demonstrated that the 3D distortion of the plasma boundary surface is enhanced with decreasing rotation speed [70]. An increase of the 3D distortion of the plasma boundary, especially near the X-point, it is not beneficial for the plasma performance since it can trigger, for example, the density pump-out, as documented in MAST [68] and in other tokamaks [69, 71, 70].

Unfortunately, none of the ELM coil control sets predicted by MARS-F modelling has been tested empirically when attempting n=2 EF control. The ELM coil control sets tested have an increased ELM coil current, in addition of having the wrong ELM coil phase alignment, for n=2 EF control. We can thus argue that the observed rotation braking is associated with the application of the non-optimal ELM coil control set for n=2 EF control.

MARS-F modelling suggests that by using $I_{ELM} = 0.2 - 0.3$ kA and $\phi_{ELM} = 100$ deg a minimization of b_{res}, in presence of plasma, both at the q=2 magnetic surface or its mean value, the rotation braking and the plasma displacement, considering various metrics, could be simultaneously achieved. By applying this model-based ELM coil control parameters an improvement of the n=2 EF control, and thus of the plasma performance, could be obtained. To test the effectiveness of MARS-F predictions on n=2 EF control, dedicated experiments have been planned in MAST-U.

It is worth stressing that this MARS-F modelling study assumes that the only source of n=2 EF in MAST-U is the one associated with P4 and P5 coil deformations, which could not be the case in the new device. To assess the importance of the n=2 EF amplitude in MAST-U, the compass scan technique will be applied at the beginning of MAST-U operation, considering the rotation sustainment as EF optimization metrics. If other potential n=2 EF sources will be identified, a model-based optimization approach, similar to the one presented here, will be adopted to tune the ELM coil control parameters for n=2 EF control.

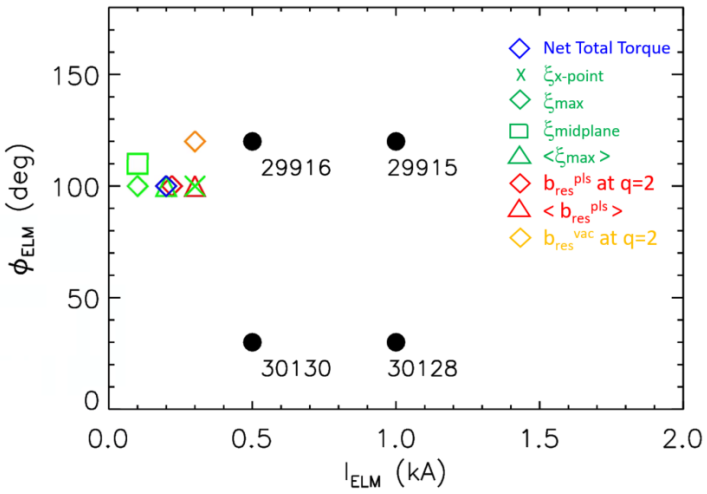

Figure 13. Control parameters for n=2 EF minimization by means of ELM coils for different n=2 EF optimization criteria. The dot symbols indicate the ELM coil control parameters tested in the experiments presented in figure 7.

5. Conclusions

This work is focused on the identification of intrinsic EF sources associated with D and P coils in MAST-U device and on the EF control strategies adopted for their minimization. The EF correction strategies have been focused on the main EF harmonics, i.e. n=1 and n=2.

In MAST-U, the static n=1 EF has been compensated by passive EF control, i.e. by finely tailoring the coil position when assembling the new device. The methodology for identifying the optimal coil position combined magnetic field measurements with 3D EM modelling and foresaw relatively small adjustment for the coil alignment, at least 3.2 mm shift and 0.7 mrad tilt in the case of P4 coil. This passive n=1 EF control strategy should guarantee no amplification of the intrinsic n=1 EF when exploring high-β regimes [22].

Conversely, the n=2 EF will be actively controlled in MAST-U. Active n=2 EF control will be mandatory in MAST-U because P4 and P5 coils, the main sources of intrinsic EFs, retained from the previous MAST device, will be fed with currents larger than the ones used in MAST when exploring various divertor configurations and high plasma current regimes.

The experience on n=2 EF control acquired during MAST operation has been of crucial importance for designing future EF control studies in MAST-U. Experiments performed in MAST, together with the corresponding MARS-F modelling, have shown that vacuum modelling is not suitable for EF control optimization, confirming findings reported in [46]. Moreover, MARS-F modelling allows the identification of a ELM coil control set which will be tested in future MAST-U n=2 EF control studies, i.e. $I_{ELM} = 0.2-0.3$ kA and $\phi_{ELM} = 100$, that should guarantee the minimization of various n=2 EF optimization criteria, i.e. b_{res} at q=2, the rotation braking and the plasma

displacement, simultaneously. The n=2 EF control strategy presented here concerns a specific plasma scenario. The model-based EF optimization approach described will be adopted also in other plasma configurations, such as the double null, where both the upper and the lower ELM coil rows will be utilized and consequenly, we foresee a different ELM coil control parameter set for n=2 EF control in this case.

It is worthwhile stressing that this study is not an exhaustive overview of all the EF sources in MAST-U, but it is focused on magnetic field errors that can be identified analysing the presently available magnetic field measurements, i.e. n=1 and n=2 harmonics. For example, the quantification of non-resonant EFs and $n > 2$ EFs is beyond the scope of this work and it will be addressed in a separate publication.

EF detection methods, such as the compass scan [51, 52], will be applied to access the importance of other potential n=1 and n=2 EF in the new device. If the n=1 and n=2 EF amplitudes have a non-negligible amplitude, active control will be applied for their correction. The multi-n EF active control schemes implemented in the PCS will use feedforward and/or dynamic current references depending on the static or dynamic EFs nature and MARS-F code will be exploited to model-based optimize the EF control parameters, using an approach similar to the one presented in this work. Other EF optimization criteria, such as the overlap criterion proposed in [48], how the EF correction will depend on plasma parameters such as the q-profile, the plasma pressure, the rotation and on the poloidal mode spectrum [44, 52] will also be considered in the future to contribute on the identification of the best EF minimization metrics towards ITER operation.

6. Acknowledgment

This work has been carried out within the framework of the EUROfusion Consortium and has received funding from the Euratom research and training programme 2014-2018 under grant agreement No 633053. The views and opinions expressed herein do not necessarily reflect those of the European Commission. This project has also received funding from the RCUK Energy Programme [grant number EP/012450/1] and it has been partly supported by US DoE Office of Science under Contract DESC0018992. To obtain further information on the data and models underlying this paper please contact PublicationsManager@ukaea.uk.

[1] Bondeson A. et al 2001 *Nucl. Fusion* **41** 455
[2] Strait E. J. et al 2004 *Phys. Plasmas* **11** 2505
[3] Evans T. E. et al 2005 *Nucl. Fusion* **45** 595
[4] Suttrop W. et al 2011 *Phys. Rev. Lett.* **106** 225004
[5] Garofalo A.M. et al 2011 *Nucl. Fusion* **51** 083018
[6] Scoville J.T. et al 1991 *Nucl. Fusion* **31** 875
[7] Buttery R.J. and Giruzzi G. 2000 *Plasma Phys. Control. Fusion*
[8] Wolfe S.M. et al 2005 *Phys. Plasmas* **12** 056110
[9] Menard J.E. et al 2010 *Nucl. Fusion* **50** 045008
[10] Boozer A.H. 2010 *Fusion Sci. and Technol.* **59** 561

[11] La Haye R.J. et al 1992 *Phys. Fluids B* **4** 2098
[12] Hender T. C. al. 1992 *Nucl. Fusion 32* 2091
[13] Buttery R.J. et al 1999 *Nucl. Fusion* **39** 1827
[14] Zhu W. et al 2006 *Phys. Rev. Lett* **96** 225002
[15] Garofalo A. M. et al 2008 *Phys. Rev. Lett* **101** 195005
[16] Frassinetti L. et al 2015 *Nucl. Fusion* **55** 112003
[17] Lazzaro E. et al 2002 *Phys. Plasmas* **9** 3906
[18] Saibene G. et al 2007 *Nucl. Fusion* **47** 969
[19] Varje J. et al 2016 *Nucl. Fusion* **56** 046014
[20] Garofalo A. et al 2012 *Nucl. Fusion* **42** 1335
[21] Sabbagh A.S. et al 2006 *Nucl. Fusion* **46** 635
[22] Igochine V. et al 2017 *Nucl. Fusion* **57**116027
[23] La Haye R.J. et al 1991 *Rev. Sci. Instrum.* **62** 2146
[24] Fishpool G. M. et al 1994 *Nucl. Fusion* **34** 109
[25] Buttery R.J. et al 2000 *Nucl. Fusion* **40** 807
[26] Lazzaro E. et al 2002 *Phys. Plasmas* **9** 3906
[27] Luxon J.L. 2002 *Nucl. Fusion* **42** 614
[28] Scoville J. T. and LaHaye R. J. 2003 *Nucl. Fusion* **43** 250
[29] Luxon J.L. et al 2003 *Nucl. Fusion* **43** 1813
[30] Wolf R. C. et al. 2005 *Nucl. Fusion***45** 1700
[31] Howell D. F. et al 2007 *Nucl. Fusion* **47** 1336
[32] Piron L. et al 2011 *Nucl. Fusion* **63** 063012
[33] Piron L. et al 2011 *Plasma Phys. Control. Fusion* **54** 084004
[34] Hu Q. M. et al 2012 *Nucl. Fusion***52** 083011
[35] Maraschek M. et al 2013 Measurement and impact of the n = 1 intrinsic error field at ASDEX Upgrade 40th EPS Conf. on Plasma Physics (Espoo, Finland, 1-5 July 2013) p P4.127 (http://ocs.ciemat.es/EPS2013PAP/pdf/P4.127.pdf)
[36] Jin W. et al. 2013 *Plasma Phys. Control. Fusion***55** 035010
[37] Volpe F.A. et al 2013 emphNucl. Fusion **53** 043018
[38] Kirk A. et al 2014 *Plasma Phys. Control. Fusion* **56** 104003
[39] Liu Y.Q. et al 2014 *Plasma Phys. Control. Fusion* **56** 104002
[40] In Y. et al 2015 *Nucl. Fusion* **55** 043004
[41] Frassinetti L. et al 2015 *Nucl. Fusion* **55** 112003
[42] Matsunaga G et al 2015 *Fusion Eng. Des.* **98** 1113-1117
[43] Wang H.Q. et al 2016 *Nucl. Fusion* **56** 0066011
[44] Wang H.H. et al 2018 *Nucl. Fusion* **58** 056024
[45] Okabayashi M. et al 2005 *Nucl. Fusion* **45** 1715-31
[46] Park J.K. et al 2007 *Phys. Rev. Lett.* **99** 195003
[47] Park J.K. et al 2009 *Phys. Plasmas* **16** 056115
[48] Park J.K. et al 2011 *Nucl. Fusion* **51** 023003
[49] Morris A. W. et al, "MAST Accomplishments and Upgrade for Fusion Next-Steps" IEEE Transactions on Plasma Science, April 2014
[50] Liu Y. Q. et al 2000 *Phys. Plasmas* **7** 3681
[51] Scoville J.T. et al 2003 *Nucl. Fusion* **43** 250
[52] Yang X. et al 2018 *Plasma Phys. Control. Fusion* **60** 055004
[53] Lanctot M.J. et al 2017 *Phys. Plasmas* 24 056117
[54] Liang Y. et al 2010 *Nucl. Fusion* **50** 025013
[55] Buttery R.J. et al 2011 *Nucl. Fusion* **51** 073016
[56] Evans T.E. et al 2006 *Nat. Phys.* **2** 419
[57] Unterberg E.A. et al 2010 *Nucl. Fusion* **50** 034011
[58] Lanctot M. J. et al 2013 *Nucl. Fusion* **53** 083019

[59] Kim K. et al 2017 *Nucl. Fusion* **57** 036014
[60] Chapman I.T. et al 2010 *Nucl. Fusion* **50** 045007
[61] Nardon E. et al 2007 *J. Nucl. Mater.* **363-365** 1071
[62] Gerhardt S.P. et al 2010 *Plasma Phys. Control. Fusion* **52** 104003
[63] Paz-Soldan C. et al 2015 *Nucl. Fusion* **55** 083012
[64] Lao L.L. et al 2005 *Fusion Sci. Technol.* **48** 968
[65] Lutjens H. et al 1996 *Computer Physics Communications* **97** 219
[66] Buttery R.J. et al 2012 *Phys. Plasmas* **19** 056111
[67] Fitzpatrick R. et al 1991 *Phys. Plasmas* **3** 664
[68] Kirk A. et al 2011 *Plasma Phys. Control. Fusion* **53** 065011
[69] Evans T. et al 2004 *Phys. Rev. Lett* **92** 235003
[70] Liu Y.Q. et al 2011 *Nucl. Fusion* **51** 083002
[71] Liang Y. et al 2007 *Phys. Rev. Lett* **98** 265004
[72] Callen J.D. 2011 *Nucl. Fusion* **51** 094026
[73] Shaing K. C et al 2010 *Nucl. Fusion* **50** 025022
[74] Rozhansky V. et al 2010 *Nucl. Fusion* **50** 034005
[75] Liu Y.Q. et al 2016 *Nucl. Fusion* **56** 066001